PHYSICAL REVIEW B VOLUME 44, NUMBER 23 15 DECEMBER 1991-I

Strain-relief mechanism in surfactant-grown epitaxial germanium films on Si(111)

F. K. LeGoues, M. Horn-Von Hoegen, M. Copel, and R. M. Tromp
IBM Research Division, Thomas J. Watson Research Center, Yorktown Heights, New York 10598
(Received 14 June 1991)

We have studied the strain-relief mechanism in Ge thin films grown on Si(111) with and without a surfactant. Films grown on bare Si tend to form islands, which results in dislocations being nucleated at numerous sites at the edges of the islands. Since the dislocations glide as Shockley partial dislocations in this system, this process generates stacking faults that thread through the film and, eventually, to the surface when the islands coalesce. When Ge is grown on an antimony-terminated Si(111) surface, the growth mode changes to a layer-by-layer mode. This forces the dislocations to nucleate at the surface. Again, Shockley partial dislocations are formed, so that, initially, a threading stacking fault extends from the surface to the interface, and then along the interface. The intersection between the surface and the threading part of the stacking fault then acts as a nucleation site for the second partial dislocation, which results in the "self-annihilation" of the threading defects. We describe relaxed Ge films on Si(111) grown by this method, as well as relaxed multilayers of the Si/Ge/Si(111) type.

I. INTRODUCTION

The Si-Ge system has received a great deal of attention, principally because of the exciting possibilities of extending the range of electronic properties that can be obtained using Si alone.[1] For example, it has recently been demonstrated that the band offset provided by small amounts of Ge in Si (below 10 at. %) can drastically increase the speed of heterojunction bipolar transistors.[2] Numerous applications have also been proposed that take advantage of the size difference between Ge and Si atoms to manipulate band gaps and offsets by "strain engineering."[1]

Most device applications for Si-Ge rely on a strained layer, matching the Si substrate by keeping the thickness of the film under a certain "critical thickness,"[3] determined by the composition. By definition, under this critical thickness, the driving force to introduce strain relieving defects in the film will be smaller than the activation barrier to either form or move the defects, keeping the film defect free throughout the processing steps necessary to obtain a device. Unfortunately, this greatly limits the range of materials, thicknesses, and thus electronic properties that can be obtained. In order to fully take advantage of the promise of the Si-Ge system, it is necessary to obtain *relaxed*, defect-free thin films. This is a very challenging problem as the strain-relief mechanism generally results in a relaxed film that contains numerous threading defects. These defects have no or little effect on the lattice parameter of the film, but are the result of the strain-relief mechanism. For example, Ge or SiGe films grown on Si(001) usually have very high densities of threading dislocations (up to $10^{12}/cm^2$). These threading dislocations are initially formed as parts of loops or half-loops. The component of these loops located at the interface is the misfit dislocation, responsible for relieving the strain. The threading part moves through the film under the influence of the stress, thus extending the misfit dislocation at the interface. In principle, the threading part of the misfit dislocation may disappear as it reaches the edge of the wafer, but this rarely occurs because the threading dislocations can become pinned by intersecting dislocations[4,5] or other defects.

Recently, we have shown[6] that the microstructure of a Ge film grown on Si(001) can be drastically altered by changing the growth mode from island growth (which is its preferred mode of growth) to layer-by-layer growth. This was achieved by using a surfactant (arsenic), which lowers the surface energy of both the Si(001) and Ge(001) surfaces.[7] The surfactant floats to the surface during growth and prevents Ge islanding. In this particular system, layer-by-layer growth delays the formation of strain-relieving defects significantly past the expected critical thickness. Indeed, the initial nucleation of dislocations is completely suppressed. Instead, so-called "V-shaped" defects are formed which relieve the misfit progressively as the film grows. Once formed, these defects serve as nucleation sites for 90° misfit dislocations which are injected into the Si substrate. Eventually, the strain is relieved both by the V-shaped defects in the Ge film and by dislocations in the Si. This demonstrates the critical importance of the growth mode in determining the strain-relief mechanism and final microstructure. Unfortunately, from a device point of view, the V-shaped defects are probably as detrimental as threading dislocations, and changing the growth mode was not enough in this case to obtain defect-free, relaxed films.

Recent experiments have shown that the surfactant technique also works for Ge growth on Si(111).[8] In this case, layer-by-layer growth is achieved by saturating the surface dangling bonds with a monolayer of antimony [one monolayer (ML) $=7.83\times10^{14}$ atoms/cm^2]. In this paper we describe the strain-relief mechanism and microstructure observed in the Si(111)/Ge/Sb system. Unlike the case of Ge on Si(001), Shockley partial dislocations[9] are introduced both with and without the Sb surfactant. However, there is a drastic difference in the *location* at which these dislocations are introduced, and this

 ©1991 The American Physical Society

results in very distinct final microstructures. In the island-growth case, dislocations glide from the edges of the islands along or near the interface. The edges of the islands provide a multitude of sites for nucleation of Shockley partial dislocations, resulting in numerous threading stacking faults when the islands finally coalesce. During layer-by-layer growth, the Shockley partial dislocation can only be introduced at the surface. The defects then thread through the film and glide along the interface. The resulting threading stacking fault acts as a nucleation site for a second Shockley partial dislocation and is annihilated as the second partial dislocation glides to the interface. This "self-annihilation" of the threading defects results in a relaxed, defect-free Ge film, with all of the strain-relieving defects located in the plane of the interface and no detectable threading defects. We have successfully used the same technique to obtain strain-relieved, defect-free multilayers of the Si(111)/Ge/Si type.

II. EXPERIMENTAL TECHNIQUE

The growth technique used in this study was described in detail in Refs. 7 and 8. Briefly, Si samples were cleaned by mild sputtering followed by a short flash at 1050 °C. Ge was deposited in UHV at 610 °C at rates of about 0.3 ML/min. The Si surface was passivated by 1 ML of Sb prior to Ge growth, and a small flux of Sb was supplied during growth. Samples were prepared for both planar-view and cross-sectional transmission-electron-microscopy (TEM) observation by mechanical thinning to about 30 μm and then ion milling to electron transparency. Samples were observed on a Philips 430 microscope operating at 300 kV and on a JEOL 4000 microscope operating at 400 kV.

III. RESULTS

A. Island growth

Figure 1 shows cross-sectional micrographs of samples grown without a surfactant. Figure 1(a) shows a coverage of about 200 ML, where large elongated islands are clearly seen. Figure 1(b) shows further growth in similar condition, where the islands have coalesced to form a continuous film. The microstructure obtained in this manner is very poor: The film is rough, and numerous threading defects are seen, mostly microtwins or stacking faults. Figure 2 shows high-resolution pictures of several

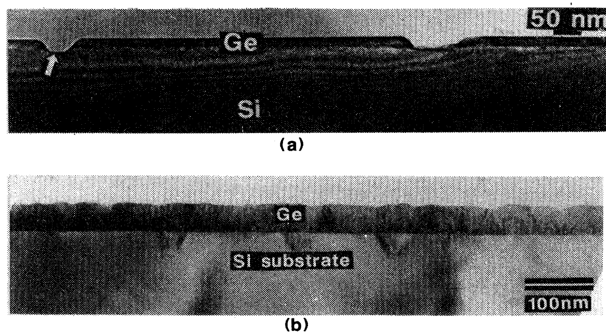

FIG. 1. Cross-sectional views of samples grown without surfactant. (a) About 200 ML. (b) After coalescence of the islands. (Note that in this case the initial growth surface was contaminated by particulates that generate stacking faults in the Si buffer layer grown prior to the Ge layer. These do generate faults in the Ge layer, but are clearly not the primary source of defects in the thin film.)

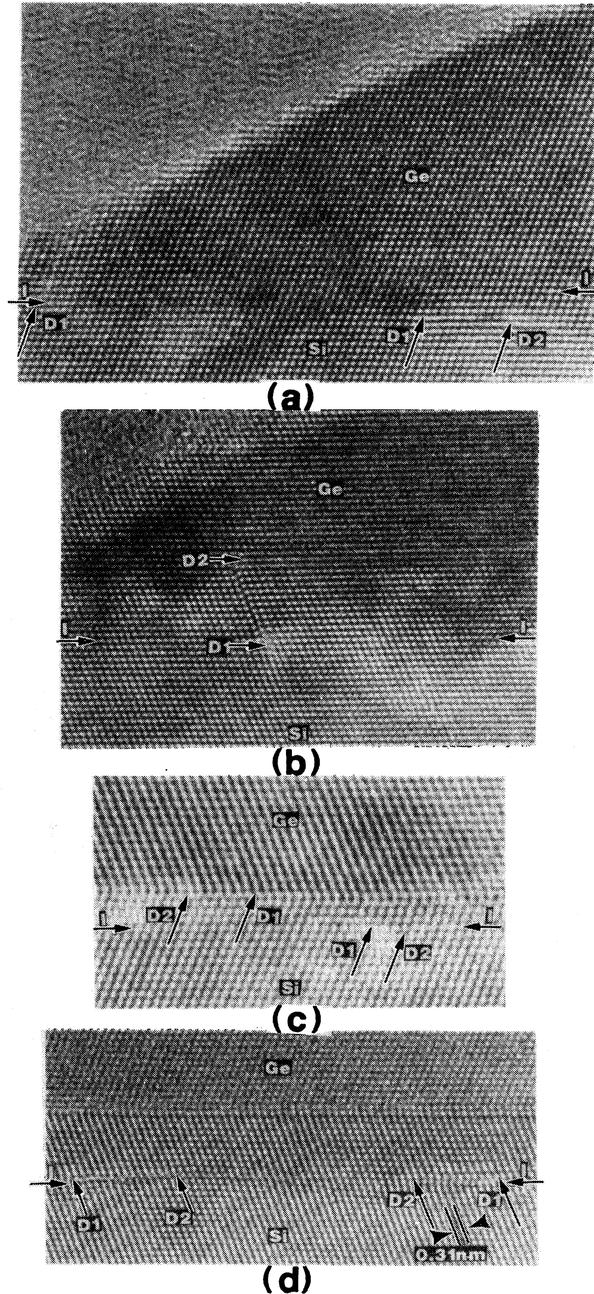

FIG. 2. High-resolution micrographs of some of the islands shown in Fig. 1(a). (a) The strain in the island is relieved by partial dislocations located in the plane of the interface, so that the island itself is defect free. (b), (c), and (d) The dislocations and associated stacking faults have generated threading defects through the islands.

islands, where strain-relieving defects are present. In Fig. 2(a) the misfit has been relieved by a series of Shockley partial dislocations[9] located on one single plane at the interface. The island in Fig. 2(a) is thus strain relieved by a network of dislocations "buried" at the interface, leaving the island itself defect free. This is unfortunately the exception. Most of the islands end up with very defective microstructures, as exemplified in Figs. 2(b)–2(d). In most cases the dislocations are not located on one single plane, but instead are spread over a large part of the thickness of the island. This results in numerous twins and stacking faults in the thin films. When the islands finally coalesce after further growth, a large proportion of these twins will thread to the surface, resulting in the defective film shown in Fig. 1(b).

B. Films grown layer by layer

Figure 3 shows the microstructure of Ge films grown with an Sb surfactant, as a function of film thickness. In Fig. 3(a), 10 ML have been deposited. The Ge film is continuous and strained, and no defects are seen. Note that this is considerably above the widely accepted thickness of 6 ML (Ref. 10) at which dislocations are expected to be introduced in this system.

In Fig. 3(b) we see that, at a thickness of 15 ML, dislocations have been introduced. The dislocations are Shockley partials with Burgers vector of the $\frac{1}{6}(2,1,1)$ type.[9] Most of them are located on the plane of the interface and thus glide on the (111) plane. Since they are imaged in a $[1\bar{1}0]$ direction, their line runs along $[1\bar{1}0]$ and they must have Burgers vectors equal to $\frac{1}{6}(1,1,-2)$ ($D1$) and $\frac{1}{6}(-1,2,-1)$ ($D2$). $D1$ denotes dislocations with Burgers vectors perpendicular to the line of the dislocation, i.e., edge dislocations, directly imaged as an extra plane in the high-resolution pictures. $D2$ denotes 30° dislocations (their Burgers vector makes a 30° angle with the line of the dislocation), which are more difficult to image and correspond on the high-resolution images to the restoration of the perfect lattice at the end of the stacking fault (see Fig. 7 and Sec. IV for details). The partial dislocations define a stacking fault located at the interface. In some cases, though, the stacking fault does not remain at the interface, but threads through the film to the surface (shown by "SF" on the micrographs). In this case only the $D1$ Shockley partial dislocation is present at the interface (a more detailed description of these dislocations will be given in Sec. IV).

Figure 3(c) shows the microstructure of a 25-ML film. Here the film itself is perfect; i.e., there are no stacking faults or other defects threading through the film. All of the strain-relieving defects are now located on one plane at the interface. These are Shockley partial dislocations again, resulting in an interface made up of alternating perfect and faulted areas. This is made clearer in Fig. 4, which shows a detail of the microstructure of about 50 ML of Ge grown layer by layer. Here, again, the Ge layer is flat and free of threading defects. All of the dislocations are located on one single atomic plane at the interface. The alternation of perfect and faulted regions has been highlighted, and the alternation of $D1$ and $D2$ Shockley partial dislocations is clearly seen.

By looking over large areas in cross section and counting the number of dislocations, we can convince ourselves that the Ge film is strain free; i.e., the Ge film has the lat-

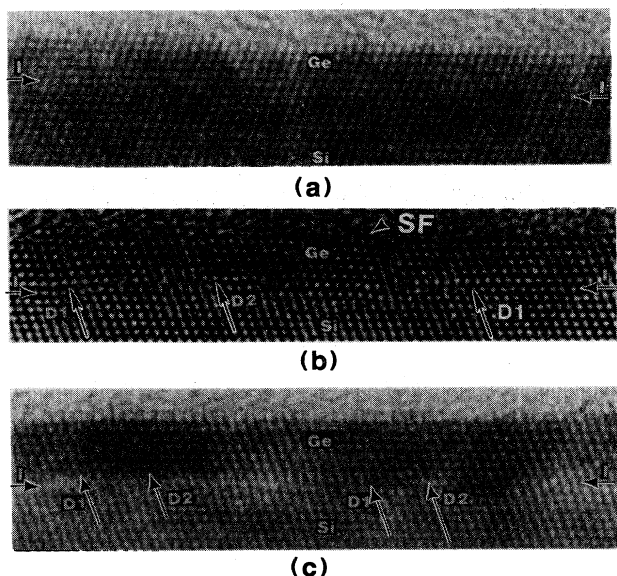

FIG. 3. Microstructure of samples grown with Sb surfactant. (a) 10 ML. (b) 15 ML. (c) 25 ML. $D1$ and $D2$ show the two partial dislocations located in the plane of the interface. "SF" shows the intersection between a threading stacking fault and surface (see text for details). I shows the plane of the interface. Note that it is not possible to exactly measure the deposited thickness on these micrographs because some of the Ge may be lost as a result of oxidation when the sample is taken out of the UHV chamber for TEM sample predation. In the case of (a), the sample was protected by a few monolayers of Si.

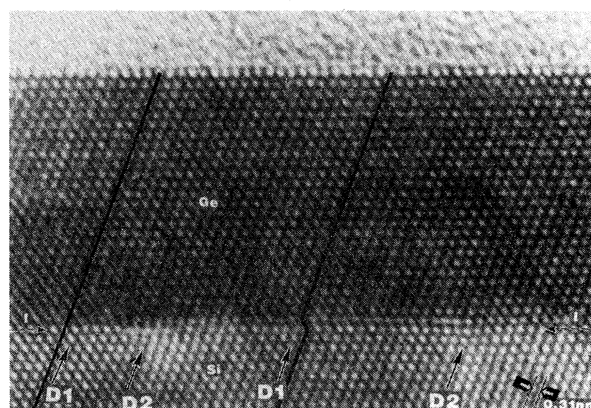

FIG. 4. High-resolution micrograph of 50 ML deposited with Sb surfactant. Note that the top layer is atomically flat. The alternation of faulted and unfaulted regions has been highlighted by following two atomic planes across the interface. Shockley partial dislocations are marked $D1$ and $D2$, respectively (see text for corresponding Burgers vectors). Arrows marked I show the plane of the interface.

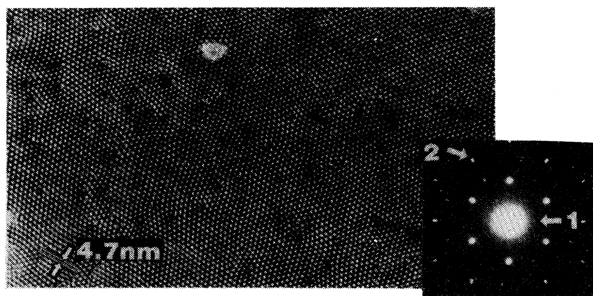

FIG. 5. Planar view and corresponding diffraction pattern of 25 ML Ge/Si(111) grown layer by layer. On the diffraction pattern, the arrow marked "1" shows extra spots at $\frac{1}{3}\{422\}$ positions. The arrow marked "2" shows the splitting of the diffraction spots resulting from the 4% lattice difference between Si and Ge.

tice parameter of bulk Ge. This corresponds to, on average, one extra plane every 25 planes. The complete relaxation is easier to determine by looking at a planar view of the film. Figure 5 shows such a micrograph. This bright-field image shows an array of moiré fringes, with a spacing of 47 Å, which corresponds to the 4% misfit between the substrate and thin film. Note that the pattern is mostly uniform, but that numerous "dislocationlike"

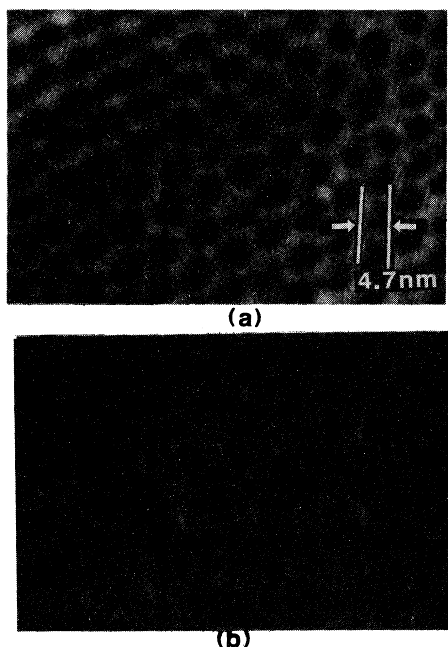

FIG. 6. (a) Bright-field planar view of 25 ML Si(111)/Ge/Si film. The moiré pattern, similar to that seen on Fig. 5, corresponds to the difference in lattice spacing between Si and Ge. (b) Dark-field planar view of the same area, obtained using one of the extra $\frac{1}{3}\{422\}$ reflections, showing an honeycomb array of stacking faults located in the plane of the interface. Note that the contrast is weak because we are imaging one single plane of atoms and because of the small size of the stacking faults.

features are imaged. These will be discussed later. The diffraction pattern also shows a 4% splitting of the diffraction spots (see arrow marked "2" on diffraction pattern). Thus, within the resolution of TEM, the Ge film is completely relaxed. The diffraction pattern shows another important feature, namely, the presence of extra reflections at $\frac{1}{3}\{422\}$ (arrow marked "1"). These arise from the presence of the fine, one-plane-thick array of stacking faults at the interface, which disrupt the diamond cubic symmetry.[11] We can image the stacking faults through dark-field imaging of these extra reflections (Fig. 6). A honeycomb array of very small (less than 50 Å) stacking faults is imaged this way.

The dense network of dislocations necessary to relieve the 4% misfit can only be imaged through the weak-beam dark-field technique.[12] In Fig. 7 weak-beam dark-field micrographs and corresponding bright-field images are

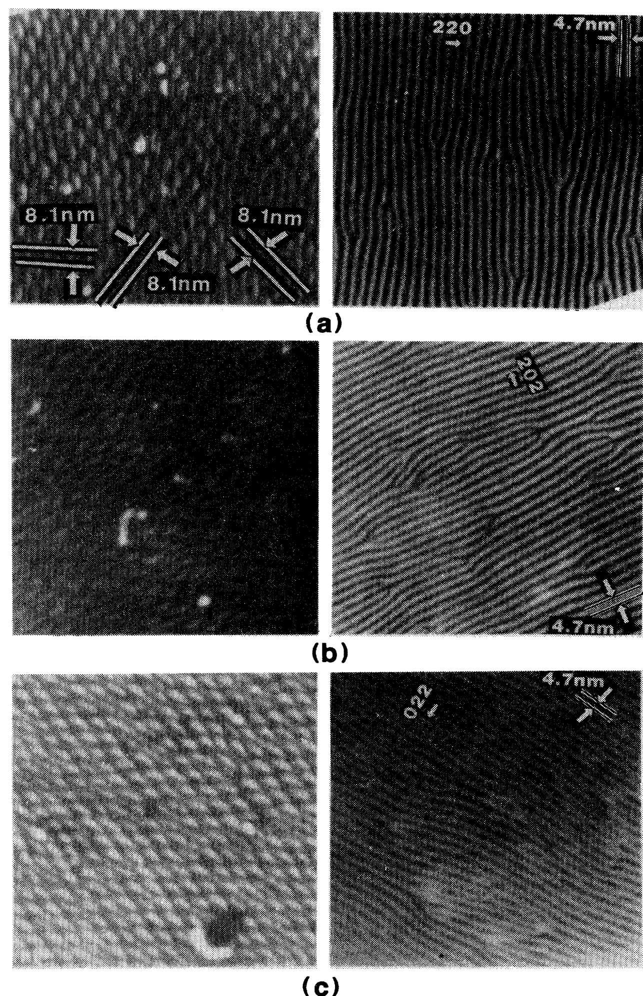

FIG. 7. Weak-beam dark-field (left) and corresponding bright-field planar views (right) of 50 ML Ge/Si(111) grown layer by layer. The bright-field images show moiré fringes corresponding to the 4% lattice misfit. (a) $\mathbf{g}=(2,-2,0)$. The spacing between the different set of visible dislocations has been highlighted for direct comparison with Fig. 8. (b) $\mathbf{g}=(2,0,-2)$. (c) $\mathbf{g}=(0,2,-2)$.

shown in three imaging directions (**g**). The bright-field images (right side of Fig. 7) show moiré fringes corresponding to the difference in lattice spacings for Si and Ge in the imaging condition. Thus a single set of moiré fringes is seen for each imaging condition, with a 47 Å spacing. Here, again, the moiré pattern is seen to contain irregularities. The weak-beam dark-field images (shown on the left side of Fig. 7) show a network of dislocations convoluted with the set of moiré fringes. These are consistent with the arrays of dislocation schematically represented in Figs. 8(a) and 8(b). These are obtained by noting that the dislocations lines run along the three equivalent ⟨110⟩ directions of the (111) plane (this is deduced directly from the high-resolution cross-sectional images and from the weak-beam dark-field images). Each set of partial dislocations is equivalent to a full edge dislocation of the $\frac{1}{2}(1,-1,0)$ type. The dislocations have to be able to glide on the plane of the interface, i.e., the (111) plane. Thus their Burgers vector must be in the plane of the interface, which means that the three sets of partial dislocations and their equivalent full dislocation must be

$$\tfrac{1}{6}(-1,-1,2)+\tfrac{1}{6}(-2,1,1)=\tfrac{1}{2}(-1,0,1)\ ,$$

$$\tfrac{1}{6}(1,1,-2)+\tfrac{1}{6}(-1,2,-1)=\tfrac{1}{2}(0,1,-1)\ ,$$

$$\tfrac{1}{6}(2,-1,-1)+\tfrac{1}{6}(1,-2,1)=\tfrac{1}{2}(1,-1,0)\ .$$

Since the equivalent $\frac{1}{2}(1,1,0)$ dislocations make a 60° angle with their dislocation line, they are only 87% [sin(60)=0.866] as effective at relieving the strain as their 90° counterparts would be. The minimum network of dislocations necessary to relieve the strain would consist of three sets of either full or partial dislocations with lines perpendicular to the three ⟨110⟩ directions of the (111) plane and with a spacing of 94 Å for full dislocations and 47 Å for partial dislocations. Instead, the lines are found to lie along ⟨110⟩, and one full dislocation (or two partial dislocations) every 81 Å [94 sin(60°)] is necessary. The orientation of the line is a direct result of the nucleation mechanism of these dislocations, which will be discussed later.

In Fig. 7, for each **g**, different **g·b** invisibility conditions apply, so that in each imaging condition different

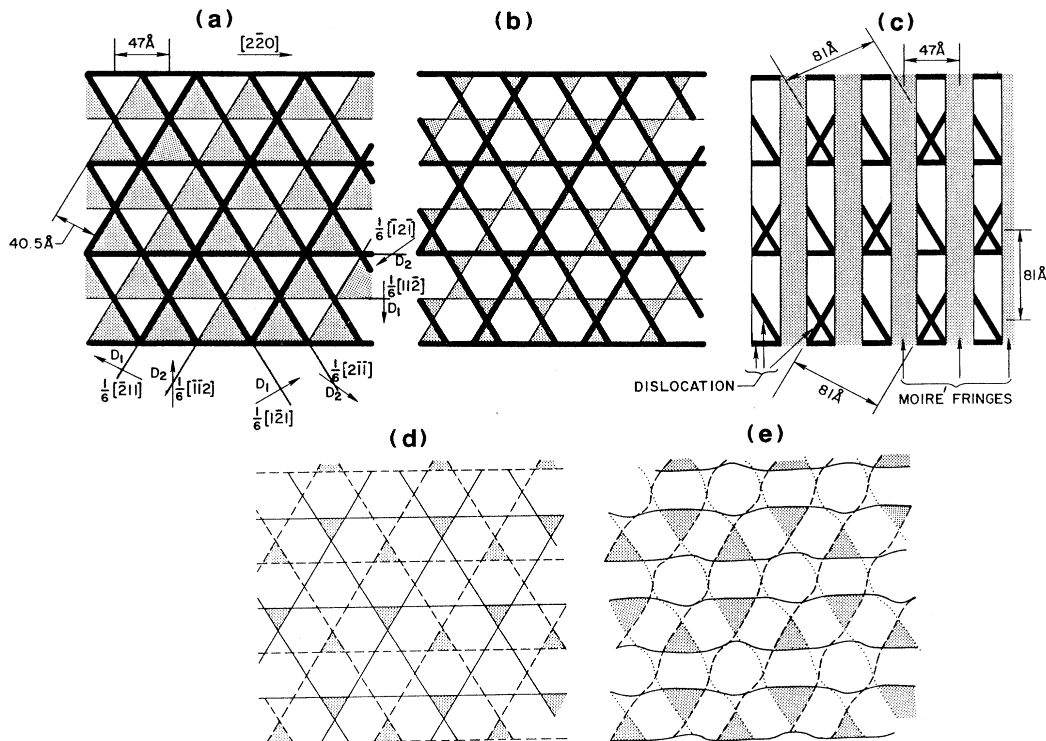

FIG. 8. (a) Schematic representation of a possible array of partial dislocations needed to relieve the misfit. The heavy lines correspond to dislocations that would be visible under the conditions of Fig. 7(a). The darkened areas correspond to the faulted regions. (b) Schematic representation of the other possible arrangement of dislocations. (c) Expected pattern resulting from the superposition of the array of dislocations highlighted in (b) with the expected set of moiré fringes. The same symmetry would result from the superposition of the array shown in (a) with the set of moiré fringes, although the exact detail of the contrast ought to be different. (d) Same dislocation network as in (b). The dashed lines represent 30° dislocations; the full lines represent 90° dislocations. Only the faults delineated by the same type of dislocations have been darkened. (e) same as (d), but the nodes highlighted in (d) have been allowed to expand. The other stacking faults are still present, but too small to be imaged.

sets of dislocations are imaged. For example, for $\mathbf{g}=(-2,2,0)$ [Fig. 7(a)], the $\mathbf{g}\cdot\mathbf{b}=0$ condition for invisibility of dislocations applies for partial dislocations with Burgers vectors along $\frac{1}{6}(1,1,-2)$, but not to those with Burgers vector along $\frac{1}{6}(-2,1,1)$ or $\frac{1}{6}(1,-2,1)$. Thus we expect to see a network consisting of two sets of dislocations 81 Å apart and one set of dislocations 40 Å apart. In Figs. 8(a) and 8(b) we have highlighted the array of dislocations that are visible in these conditions, and in Fig. 8(c) we show the pattern resulting from the convolution of the array of dislocations with the set of moiré fringes. The exact contrast expected from such a dense network of dislocations would be very difficult to calculate. Thus only the symmetry of the expected pattern is revealed in Fig. 8(c). The same symmetry is expected for the configuration shown in Fig. 8(b). Note that it corresponds exactly to the pattern shown in Fig. 7(a). The same reasoning applies for Figs. 7(b) and 7(c).

IV. DISCUSSION

In this system the growth mode is a dominant factor in determining the final microstructure of the film. Instead of a rough, highly defected film obtained with island growth (Fig. 1), in layer-by-layer growth we are now able to obtain films where all of the strain-relieving defects are located on one single plane at the interface, leaving the Ge film relaxed and defect free. This is achieved by changing the location at which dislocations are nucleated. Under conventional growth conditions, edges of islands provide numerous low-energy nucleation sites for dislocation formation. Since (111) planes are the preferred glide planes for dislocations in Si and Ge, dislocations that are nucleated anywhere at the edge of an island can glide toward the center of the island. But the dislocations tend to nucleate and glide as Shockley partial dislocations, leaving a stacking fault behind. If a second partial dislocation then glides on the exact same plane, it will annihilate the stacking fault and restore the perfect lattice. In the case of islands, this is very unlikely because of the plethora of nucleation sites: Dislocations will tend to nucleate near the interface, but unless they are on exactly the same plane, they will leave a high density of stacking fault in the islands. Figure 9 illustrates this point. The side of an island is shown, where several stacking faults have glided from the edge, covering a thickness of about 100 Å. This results in the defective structures shown in Figs. 2(b)–2(d).

On the other hand, during layer-by-layer growth, dislocations can only nucleate at the surface. This is clearly difficult and results in delayed nucleation; i.e., a strained film can be grown to a larger thickness before defects are introduced [Fig. 3(a)]. Even though the dislocations have to nucleate at the surface, we find that, at the end, the microstructure consists of an array of dislocations exclusively located on the plane of the interface. Let us consider the case of the one set of partial dislocations that is equivalent to the full dislocation with Burgers vector equal to $\frac{1}{6}(1,0,-1)$ and which can glide on (111):

$$\tfrac{1}{2}(1,0,-1)=\tfrac{1}{6}(1,1,-2)+\tfrac{1}{6}(2,-1,-1)\ .$$

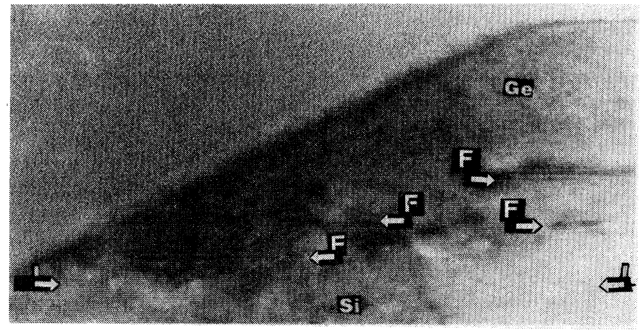

FIG. 9. High-resolution cross-sectional view of the edge of a Ge island showing that dislocations have glided at different depths. *I* shows the plane of the interface. The arrows marked *F* indicate different stacking faults.

Neither the full dislocation nor the partial dislocations can nucleate during layer-by-layer growth since they are only mobile on the plane of the interface. Thus this final set of dislocations can only have evolved from the reaction between dislocations that can be nucleated, i.e., dislocations that can glide to the interface along $(11\bar{1})$, $(1\bar{1}1)$, or $(\bar{1}11)$. Figure 10(a) shows a schematic representation of the total dislocation reaction that has to happen in this case. The inset in Fig. 10(a) shows the atomic arrangement and the involved Burgers vectors in a $[1\bar{1}0]$ projection. The line of the dislocation is perpendicular to this projection, i.e., the line lies along $[1\bar{1}0]$. The full interfacial dislocation can be dissociated as two other full dislocations, one that can glide on the $(11\bar{1})$ plane $[\mathbf{b}=\frac{1}{2}(0,-1,-1)]$ and a sessile edge dislocation with $\mathbf{b}=\frac{1}{2}(1,1,0)$. Thus the $\frac{1}{2}(0,-1,-1)$ dislocation can glide from the surface to the interface, then cross slip onto the plane of the interface. The cross-slip reaction results in the formation of the $\frac{1}{2}(1,1,0)$ edge dislocation that can then climb to the surface, which removes the "excess atoms" in the Ge film.

This mechanism cannot happen as one step though, because the $\frac{1}{2}(0,-1,-1)$ dislocation forms at partial dislocations, probably because of the lower activation barrier associated with the nucleation of the partial dislocation:

$$\tfrac{1}{2}(0,-1,-1)=\tfrac{1}{6}(-1,-1,-2)+\tfrac{1}{6}(1,-2,-1)\ .$$

The first partial dislocation to nucleate will be the one associated with the highest amount of strain relief (which is equivalent to the largest driving force for nucleation), i.e., the one whose Burgers vector has the largest edge component in the (111) plane. In this case its Burgers vector will be equal to $\frac{1}{6}(-1,-1,-2)$ with a line along $[1\bar{1}0]$. As it glides to the interface, this dislocation generates a stacking fault on the $(11\bar{1})$ plane. As it reaches the interface, it will cross slip onto the (111) plane, forming a 90° dislocation in the plane of the interface, with a Burgers vector equal to $\frac{1}{6}(1,1,-2)$. This reaction results in the formation of a "stair-rod"[13] dislocation at the intersection between the threading and interfacial stacking faults, with a Burgers vector equal to the difference between the Burgers vector of the initial dislocation and the interfa-

cial dislocation, i.e., $\frac{1}{3}(-1,-1,0)$. This is the point at which we observe the system in Fig. 3(b) and, in closer detail, in Fig. 10(b). Here we clearly see the interfacial as well as the threading stacking fault and the resulting 90° dislocation at the interface.

This microstructure must be stable for a few monolayers because a second nucleation event is necessary in order to change it: It involves the formation of the second Shockley partial dislocation $[\mathbf{b}=\frac{1}{6}(1,-2,-1)]$ and its glide from the surface to the interface. The driving force for nucleating this partial dislocation is again the strain in the film. Unlike the island case, here the only preferential nucleation site is the intersection between the surface and threading partial dislocation; thus the second partial dislocation will glide on the exact same plane as the first one, annihilating the threading stacking fault. As it reaches the interface, it reacts with the stair-rod dislocation to form the second interfacial partial dislocation $[\mathbf{b}=\frac{1}{6}(2,-1,-1)]$ and a sessile edge dislocation with $\mathbf{b}=\frac{1}{2}(0,-1,-1)$. This dislocation then climbs to the surface, leaving the Ge film defect free and relaxed by an array of dislocations completely localized in the plane of the interface.

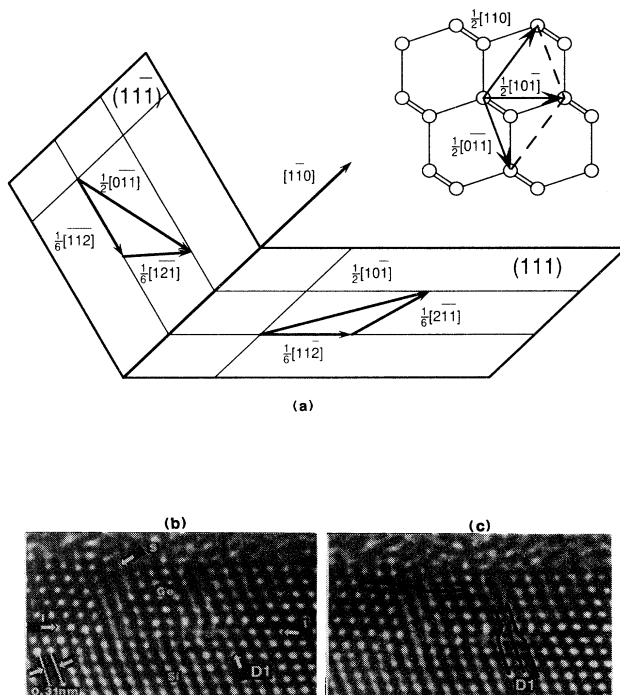

FIG. 10. (a) Schematic representation of the planes along which dislocations glide during formation of the final array. The lines of the dislocations and their orientation relative to the Burgers vector involved is shown. The inset shows the atomic arrangement in this projection and the Burgers vector of the full dislocations. (b) Detail of Fig. 2(b), showing the atomic arrangement in the 15 ML Ge film. The arrow marked *I* shows the plane of the interface. The arrow marked *S* shows the intersection between the threading stacking fault and surface. The arrow marked *D*1 shows the partial dislocation generated at the interface. (c) Same image, with atomic position superimposed. The partial dislocation (*D*1) has been highlighted, as well as the threading staking fault in the Ge film.

What is truly outstanding is the efficiency of the annihilation of the threading stacking faults. Through extensive investigation of several cross-sectional samples, not a single threading stacking fault was found in the thickest sample (Fig. 4). We attribute this to the difficulty in nucleation dislocations. Indeed, in this case, the intersections of the stacking faults with the surface of the film are the only possible nucleation sites. In this manner a strain-relieved, defect-free film can be achieved by "self-annihilation" of the threading defects formed during the initial stages of strain relaxation. Considering that the initial partial dislocations have to form as half-loops from the surface, it is rather surprising that no threading partial screw dislocations (i.e., the edges of the half-loops) is seen after the relaxation is complete. This is easy to explain, though, by considering the very high density of partial dislocations that have to be generated: Since one partial dislocation has to be present every 40 Å, it is statistically very likely that most half-loops formed will react with intersecting half-loops of the same nature (which results in the annihilation of the threading parts) without having to extend past a few hundred angstroms at the most. This is in fact made significantly easier by the fact that all the dislocations glide on the (111) plane, and the threading parts attract each other; thus two dislocations in the proximity of each other will tend to meander to form one single dislocation, annihilating the threading parts. By the same token, though, it is unlikely that a perfect dislocation network can be achieved. The dislocation lines are expected to meander significantly in order to form a continuous network. In Ref. 6, where a similar network of dislocations was obtained for a (001) interface, it was possible to image directly the dislocations because they were significantly farther apart than in the present case. There, the network appeared to meander considerably, probably in order to annihilate complementary threading dislocations and thus reduce the total energy of the interface. Similar meandering is expected for the present interface. Further, it is likely that the alternation of 30° and 90° dislocations is not perfect and that some of the partial dislocations have collapsed to form full dislocations. All of these irregularities can explain the appearance of the moiré pattern, which shows apparent "dislocations." As pointed out by Hirsh *et al.*,[14] an apparent dislocation in a moiré pattern can directly be interpreted as a dislocation in either the substrate, the overlayer, or at the interface. When the simple case of a dislocation perpendicular (or nearly perpendicular) to the film is treated, it is very easy to relate the position and apparent Burgers vector of the dislocation in the moiré pattern to that in the thin films. Unfortunately, if the direction of the line has an appreciable projected length in the image, the apparent dislocation in the moiré pattern cannot be related to the position of the dislocation itself, and the Burgers vector has to be taken along the whole line of the projected length of the dislocation. For the present case, where a very dense network of

dislocations runs parallel to the plane of the image, the moiré pattern cannot be directly interpreted. It probably reflects all of the possible irregularities in the dislocation network outlined above as well as dislocation reactions between the three sets of dislocations at the interface. As long as such a dislocation reaction does not change the total Burgers vector, no threading dislocation will result, but an apparent dislocation may appear in the moiré pattern. Some of the apparent dislocations may also be due to threading dislocations, but it is not possible to determine which one or even how many. Thus, in order to obtain a defect count, we can only rely on the results obtained from the cross-sectional views. In this way an upper limit of $10^8/\text{cm}^2$ for threading dislocation is reached. Note that the actual number may be significantly smaller than this. Also, note that this clearly demonstrates that all of the apparent defects imaged in the planar view cannot possibly be threading dislocations. Indeed, if this were the case, a dislocation density of more that $10^{11}/\text{cm}^2$ would be obtained, so that it would be impossible to image any cross section without showing several threading dislocations.

The relaxation mechanism results in the array of stacking faults located in the plane of the interface imaged in Fig. 6(b). The honeycomb pattern closely resembles that shown schematically in Fig. 8(b). We note, though, that the size of the imaged honeycomb pattern is twice that shown in Fig. 8(b). This may be attributed to the fact that all of the dislocations nodes (we define nodes as intersections of three dislocations, resulting in the formation of a triangular stacking fault) formed by the intersecting dislocations are not equivalent and thus not expected to have the same energy. Although it is very difficult to calculate (or even estimate) the energy of such a complicated array of dislocations, it is obvious that some nodes will tend to expend (the ones between dislocations that repel each other most strongly) and some will tend to contract. In Fig. 8(d) we have highlighted equivalent nodes (i.e., nodes consisting exclusively of 90° dislocations and nodes consisting exclusively of 30° dislocations, but not "mixed" nodes). These define a honeycomb pattern twice the size of the original one. If we assume that these would expand at the detriment of the other ones, we obtain the configuration shown in Fig. 6(b) and illustrated in Fig. 8(e). Note that this mechanism disrupts the dislocation network very lightly, so that the arguments used to interpret Fig. 7 are still valid.

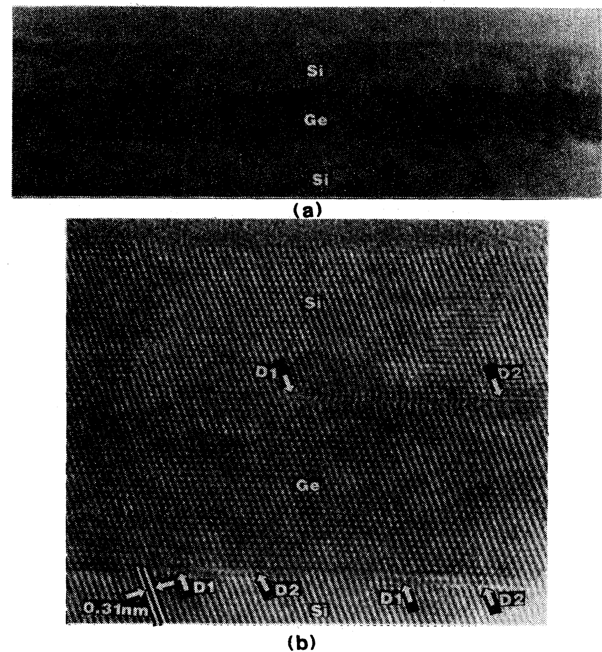

FIG. 11. High-resolution micrographs of a Si/Ge/Si(111) multilayer grown using the surfactant technique. (a) Wide area. (b) Higher magnification, showing the atomic arrangement. Equivalent but inverse dislocations are at both interfaces.

V. CONCLUSIONS

We have shown that relaxed, perfect films can be grown by changing the growth mode of Ge on Si(111) from an island type to a layer-by-layer type growth. As was discussed in Ref. 6, the dominant parameter is the control of nucleation sites for strain-relieving defects. By forcing dislocations to nucleate at the surface, we were able to grow strain-free, defect-free thin films. Once a relaxed Ge layer has been grown, the same technique can be used to grow a multilayer structure. Figure 11 shows a relaxed Ge layer sandwiched between the Si substrate and a relaxed Si layer. The same relaxation mechanism has occurred at the second Ge/Si interface. In effect, the Ge film now behaves as a perfect Ge substrate. This could be repeated as needed to obtain any type of multilayer.

---

[1] *Heterostructures on Silicon: One Step Further with Silicon*, edited by Y. I. Nissin and E. Rosencher (Kluwer, Dordrecht, 1989).

[2] G. L. Patton, J. H. Comfort, B. S. Meyerson, E. F. Crabbe, G. J. Scilla, E. DeFresart, J. M. C. Stork, J. Y.-C. Sun, D. L. Harame, and J. Burghartz, Electron Device Lett. **11**, 171 (1990).

[3] J. W. Matthews and A. E. Blakeslee, J. Cryst. Growth **29**, 273 (1975).

[4] R. Hull, J. C. Bean, and C. Buescher, J. Appl. Phys. **66**, 5837 (1989).

[5] L. B. Freund, J. Appl. Phys. **68**, 2073 (1990).

[6] F. K. LeGoues, M. Copel, and R. Tromp, Phys. Rev. B **42**, 11 690 (1990).

[7] M. Copel, M. C. Reuter, E. Kaxiras, and R. M. Tromp, Phys. Rev. Lett. **63**, 632 (1989).

[8] M. Horn-von Hoegen, F. K. LeGoues, M. Copel, and R. Tromp, Phys. Rev. Lett. **67**, 1130 (1991).

[9] Full lattice dislocations in Si and Ge generally have a Burgers vector of the $\frac{1}{2}(1,1,0)$ type, which can most easily glide on

the $(1\bar{1}1)$ plane. However, because of the low energy associated with stacking faults in Si and Ge, these dislocations will often dissociate as Shockley partial dislocations, leaving a faulted region between the two partial dislocations on the $(1\bar{1}1)$ plane. A complete description of this mechanism can be found in *Theory of Dislocations,* 2nd. ed., edited by J. P. Hirthe and J. Lothe (Wiley, New York, 1982), Chap. 10.

[10]J. Bevk, J. P. Mannaerts, L. C. Feldman, B. A. Davidson, and A. Ourmazd, Appl. Phys. Lett. **49**, 286 (1986).

[11]A. Ourmazd, G. D. Anstis, and P. B. Hirsch, Philos. Mag. **48**, 139 (1983).

[12]I. L. F. Ray and D. J. H. Cockayne, Proc. R. Soc. London Ser. A **325**, 543 (1971).

[13]"Stair-rods" dislocations are formed when two Shockley partial dislocations on two different $\{111\}$ planes interact. Here a $\frac{1}{6}(1,1,-2)$ dislocation ($D1$ in Figs. 2, 3, 4, and 10) is formed when either a $\frac{1}{6}(1,1,2)$ or a $\frac{1}{6}(-1,-1,-2)$ has glided to this interface. Since the total Burgers vector has to remain constant, this means that another dislocation (called "stair-rod") has to be generated at the intersection between the two stacking faults. The Burgers vector of the new dislocation will be the difference between the Burgers vector of the two Shockley partial dislocations involved in the reaction, i.e., $\mathbf{b}=\frac{1}{3}(0,0,-2)$ or $\mathbf{b}=\frac{1}{3}(1,1,0)$; see *Theory of Dislocations* (Ref. 9), Chap. 10, for a complete discussion of this mechanism.

[14]P. Hirsch, A. Howie, R. B. Nicholson, D. W. Pashley, and M. J. Whelan, in *Electron Microscopy of Thin Crystals,* 2nd ed., edited by P. Hirsch and A. Howie (Krieger, Malabar, FL, 1977), Chap. 15.

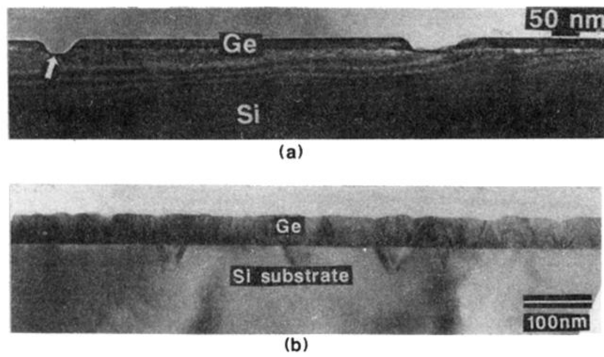

FIG. 1. Cross-sectional views of samples grown without surfactant. (a) About 200 ML. (b) After coalescence of the islands. (Note that in this case the initial growth surface was contaminated by particulates that generate stacking faults in the Si buffer layer grown prior to the Ge layer. These do generate faults in the Ge layer, but are clearly not the primary source of defects in the thin film.)

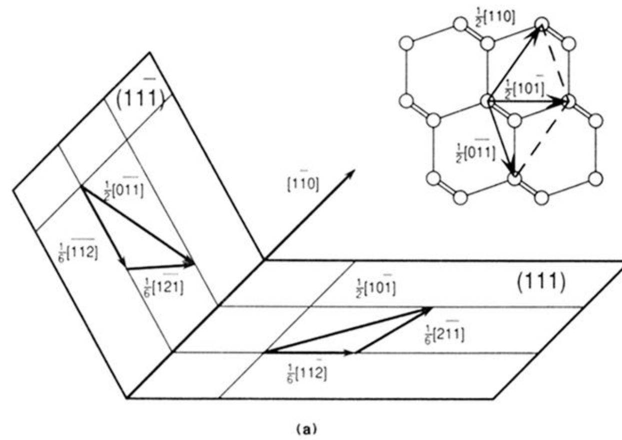

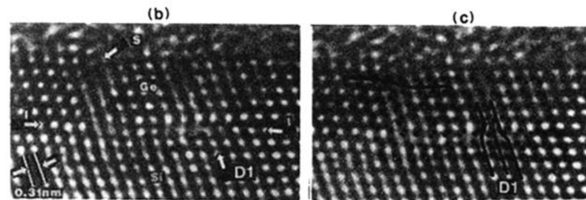

FIG. 10. (a) Schematic representation of the planes along which dislocations glide during formation of the final array. The lines of the dislocations and their orientation relative to the Burgers vector involved is shown. The inset shows the atomic arrangement in this projection and the Burgers vector of the full dislocations. (b) Detail of Fig. 2(b), showing the atomic arrangement in the 15 ML Ge film. The arrow marked I shows the plane of the interface. The arrow marked S shows the intersection between the threading stacking fault and surface. The arrow marked $D1$ shows the partial dislocation generated at the interface. (c) Same image, with atomic position superimposed. The partial dislocation ($D1$) has been highlighted, as well as the threading staking fault in the Ge film.

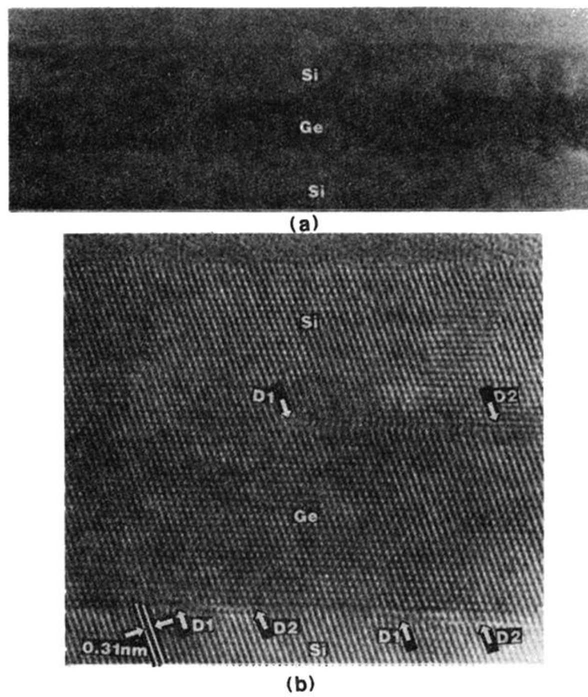

FIG. 11. High-resolution micrographs of a Si/Ge/Si(111) multilayer grown using the surfactant technique. (a) Wide area. (b) Higher magnification, showing the atomic arrangement. Equivalent but inverse dislocations are at both interfaces.

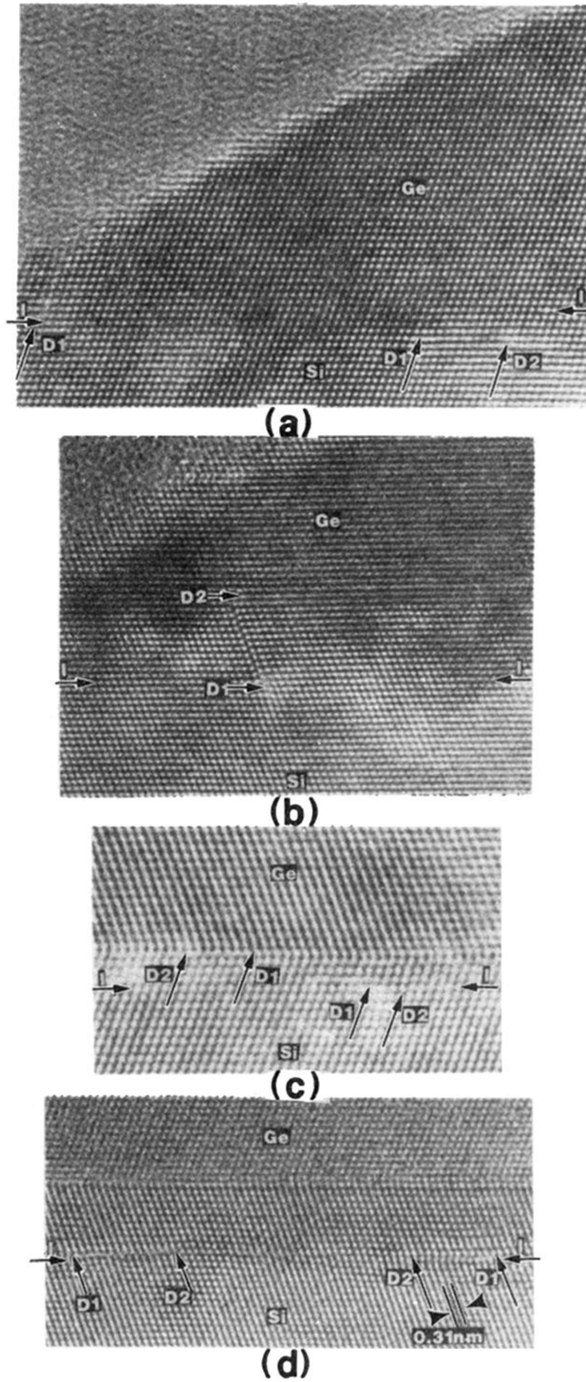

FIG. 2. High-resolution micrographs of some of the islands shown in Fig. 1(a). (a) The strain in the island is relieved by partial dislocations located in the plane of the interface, so that the island itself is defect free. (b), (c), and (d) The dislocations and associated stacking faults have generated threading defects through the islands.

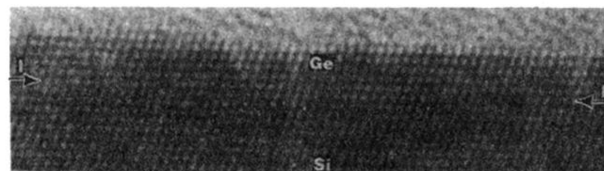

(a)

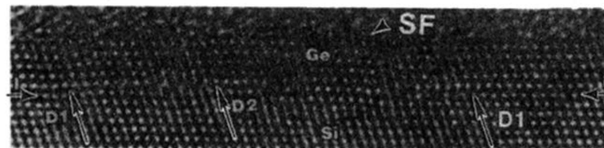

(b)

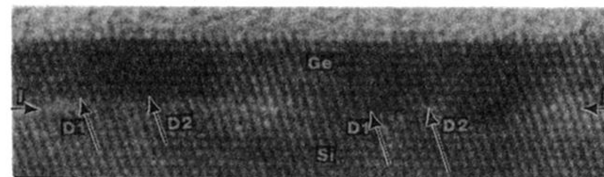

(c)

FIG. 3. Microstructure of samples grown with Sb surfactant. (a) 10 ML. (b) 15 ML. (c) 25 ML. $D1$ and $D2$ show the two partial dislocations located in the plane of the interface. "SF" shows the intersection between a threading stacking fault and surface (see text for details). I shows the plane of the interface. Note that it is not possible to exactly measure the deposited thickness on these micrographs because some of the Ge may be lost as a result of oxidation when the sample is taken out of the UHV chamber for TEM sample predation. In the case of (a), the sample was protected by a few monolayers of Si.

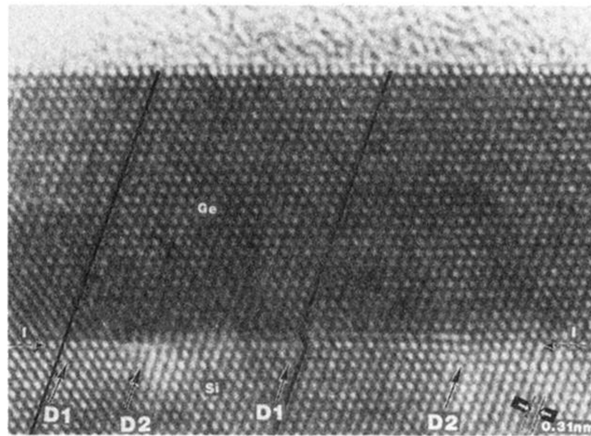

FIG. 4. High-resolution micrograph of 50 ML deposited with Sb surfactant. Note that the top layer is atomically flat. The alternation of faulted and unfaulted regions has been highlighted by following two atomic planes across the interface. Shockley partial dislocations are marked $D1$ and $D2$, respectively (see text for corresponding Burgers vectors). Arrows marked I show the plane of the interface.

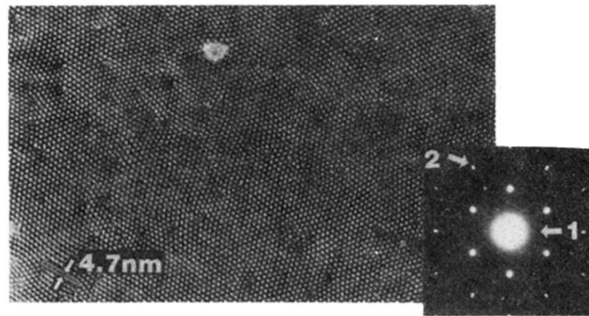

FIG. 5. Planar view and corresponding diffraction pattern of 25 ML Ge/Si(111) grown layer by layer. On the diffraction pattern, the arrow marked "1" shows extra spots at $\frac{1}{3}\{422\}$ positions. The arrow marked "2" shows the splitting of the diffraction spots resulting from the 4% lattice difference between Si and Ge.

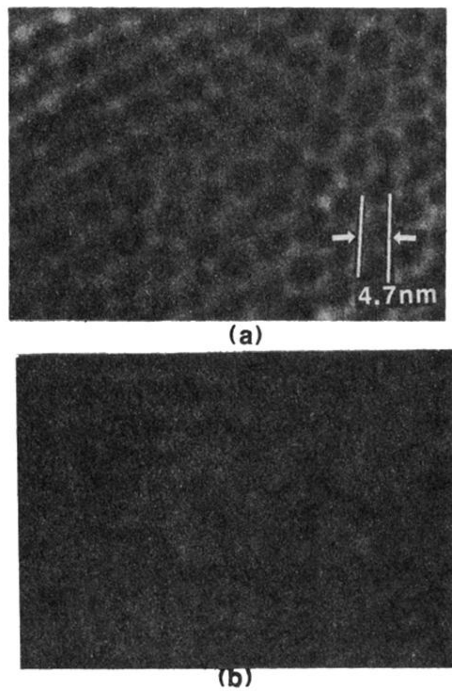

FIG. 6. (a) Bright-field planar view of 25 ML Si(111)/Ge/Si film. The moiré pattern, similar to that seen on Fig. 5, corresponds to the difference in lattice spacing between Si and Ge. (b) Dark-field planar view of the same area, obtained using one of the extra $\frac{1}{3}\{422\}$ reflections, showing an honeycomb array of stacking faults located in the plane of the interface. Note that the contrast is weak because we are imaging one single plane of atoms and because of the small size of the stacking faults.

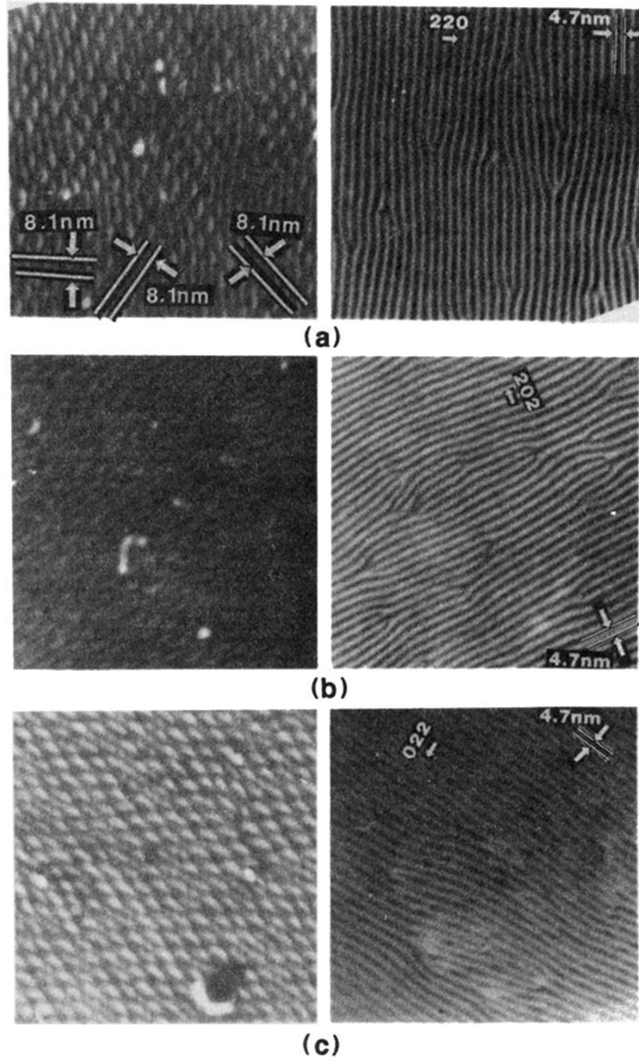

FIG. 7. Weak-beam dark-field (left) and corresponding bright-field planar views (right) of 50 ML Ge/Si(111) grown layer by layer. The bright-field images show moiré fringes corresponding to the 4% lattice misfit. (a) $\mathbf{g}=(2,-2,0)$. The spacing between the different set of visible dislocations has been highlighted for direct comparison with Fig. 8. (b) $\mathbf{g}=(2,0,-2)$. (c) $\mathbf{g}=(0,2,-2)$.

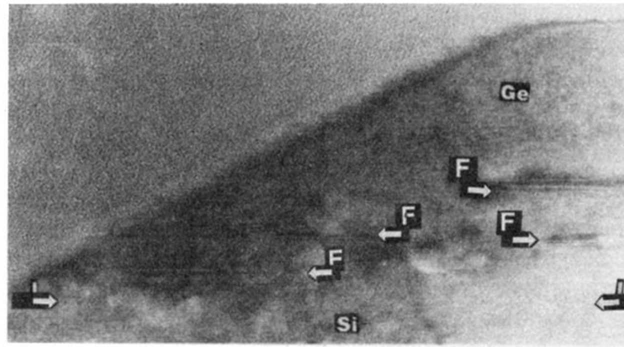

FIG. 9. High-resolution cross-sectional view of the edge of a Ge island showing that dislocations have glided at different depths. *I* shows the plane of the interface. The arrows marked *F* indicate different stacking faults.